Accelerated Article Preview

Chloroquine does not inhibit infection of human lung cells with SARS-CoV-2

Markus Hoffmann, Kirstin Mösbauer, Heike Hofmann-Winkler, Artur Kaul, Hannah Kleine-Weber, Nadine Krüger, Nils C. Gassen, Marcel A. Müller, Christian Drosten & Stefan Pöhlmann

Article

Chloroquine does not inhibit infection of human lung cells with SARS-CoV-2

Markus Hoffmann[1,2 ✉], Kirstin Mösbauer[3,4], Heike Hofmann-Winkler[1], Artur Kaul[1], Hannah Kleine-Weber[1,2], Nadine Krüger[1], Nils C. Gassen[5], Marcel A. Müller[3,4,6], Christian Drosten[3,4] & Stefan Pöhlmann[1,2 ✉]

The COVID-19 pandemic, which is caused by the novel coronavirus SARS-CoV-2, has been associated with more than 470,000 fatal cases worldwide. In order to develop antiviral interventions quickly, drugs used for treatment of unrelated diseases are currently being repurposed to combat COVID-19. Chloroquine is a anti-malaria drug that is frequently employed for COVID-19 treatment since it inhibits SARS-CoV-2 spread in the kidney-derived cell line Vero[1–3]. Here, we show that engineered expression of TMPRSS2, a cellular protease that activates SARS-CoV-2 for entry into lung cells[4], renders SARS-CoV-2 infection of Vero cells insensitive to chloroquine. Moreover, we report that chloroquine does not block SARS-CoV-2 infection of the TMPRSS2-positive lung cell line Calu-3. These results indicate that chloroquine targets a pathway for viral activation that is not operative in lung cells and is unlikely to protect against SARS-CoV-2 spread in and between patients.

Chloroquine and hydroxychloroquine are used for Malaria treatment and have been widely employed to treat COVID-19 patients, with more than 80 registered clinical trials worldwide[2,3]. Chloroquine and hydroxychloroquine inhibit SARS-CoV-2 infection of Vero cells[1,5,6], providing a rational for using these drugs for COVID-19 treatment. However, it is unknown whether these drugs inhibit infection of lung cells and it is poorly understood how they inhibit SARS-CoV-2 infection.

Chloroquine and hydroxychloroquine elevate endosomal pH and inhibit viruses that depend on low pH for cell entry[7]. We asked whether they also block SARS-CoV-2 cell entry and whether entry inhibition accounts for blockade of SARS-CoV-2 infection. Moreover, we investigated whether entry inhibition is cell type-dependent, since the virus can employ pH-dependent and pH-independent pathways for entry into cells. Thus, SARS-CoV-2 spike protein (SARS-2-S), which mediates viral entry, is activated by the endosomal pH-dependent cysteine protease cathepsin L (CatL) in certain cell lines[4]. In contrast, entry into airway epithelial cells, which express low levels of CatL[8], depends on the pH-independent, plasma membrane resident serine protease TMPRSS2[4]. Importantly, CatL usage by coronaviruses is restricted to cell lines[8–10] while TMPRSS2 activity is essential for viral spread and pathogenesis in the infected host[11,12].

We compared chloroquine and hydroxychloroquine-mediated inhibition of SARS-2-S-mediated entry into Vero (kidney), Vero-TMPRSS2 and Calu-3 (lung) cells. Calu-3 cells, like airway epithelium, express low amounts of CatL[8] and SARS-CoV-2 entry into these cells is TMPRSS2-dependent[4]. In contrast, Vero cell entry of SARS-CoV-2 is CatL-dependent while both CatL and TMPRSS2 support entry into Vero-TMPRSS2 cells[4]. As control, we used camostat mesylate, which inhibits TMPRSS2-dependent entry[4].

Camostat mesylate treatment did not interfere with cell viability while chloroquine and hydroxychloroquine slightly reduced viability when applied at the highest concentration (Fig. 1a). Inhibition of SARS-2-S-driven entry by camostat mesylate was only observed with TMPRSS2^{+} cell lines, as expected (Fig. 1a, Table 1). Moreover, chloroquine and hydroxychloroquine inhibited SARS-2-S-driven entry into Vero cells (TMPRSS2^{-}) with high efficiency while inhibition of entry into Calu-3 and Vero-TMPRSS2 (both TMPRSS2^{+}) cells was inefficient or absent, respectively (Fig. 1a, Table 1). Thus, chloroquine and hydroxychloroquine can block SARS-2-S-driven entry but inhibition is cell line-dependent and efficient inhibition is not observed with TMPRSS2^{+} lung cells.

We next investigated whether the cell type-dependent differences in entry inhibition translated into differential inhibition of authentic SARS-CoV-2. Indeed, chloroquine efficiently blocked SARS-CoV-2 infection of Vero kidney cells, as expected[1], but failed to efficiently inhibit SARS-CoV-2 infection of Calu-3 lung cells (Fig. 1b, c). A subtle reduction in SARS-CoV-2 infection was seen in the presence of 100 µM chloroquine, in keeping with the modest inhibition of pseudotype entry under those conditions (Fig. 1a), but this effect was not statistically significant. In sum, chloroquine failed to efficiently block Calu-3 cell infection with SARS-2-S-bearing pseudotypes and authentic SARS-CoV-2, indicating that in these cells chloroquine does not appreciably interfere with viral entry or the subsequent steps of the viral replication cycle.

Confirmation of our results with primary respiratory epithelium is pending. Moreover, we note that virus production in Calu-3 relative to Vero E6 cells was more robust in the present study as compared to a published one[13], potentially due to use of the Calu-3 subclone 2B4 in the previous but not the present study. Nevertheless, our results suggest that chloroquine and hydroxychloroquine will exert no antiviral

[1]Deutsches Primatenzentrum – Leibniz Institute for Primate Research, Göttingen, Germany. [2]Faculty of Biology and Psychology, Georg-August-University Göttingen, Göttingen, Germany. [3]Charité-Universitätsmedizin Berlin, corporate member of Freie Universität Berlin, Humboldt-Universität zu Berlin, and Berlin Institute of Health, Institute of Virology, Berlin, Germany. [4]German Centre for Infection Research, associated partner Charité, Berlin, Germany. [5]Department of Psychiatry and Psychotherapy, University of Bonn, 53127, Bonn, Germany. [6]Martsinovsky Institute of Medical Parasitology, Tropical and Vector Borne Diseases, Sechenov University, Moscow, Russia. ✉e-mail: mhoffmann@dpz.eu; spoehlmann@dpz.eu

Article

activity in human lung tissue and will not be effective against COVID-19, in keeping with the results of recent clinical trials[14,15]. Moreover, they highlight that cell lines mimicking important aspects of respiratory epithelial cells should be used when analyzing the antiviral activity of drugs targeting host cell functions.

Online content

Any methods, additional references, Nature Research reporting summaries, source data, extended data, supplementary information, acknowledgements, peer review information; details of author contributions and competing interests; and statements of data and code availability are available at https://doi.org/10.1038/s41586-020-2575-3.

1. Wang, M. et al. Remdesivir and chloroquine effectively inhibit the recently emerged novel coronavirus (2019-nCoV) in vitro. Cell Res 30, 269-271, https://doi.org/10.1038/s41422-020-0282-0 (2020).
2. Ferner, R. E. & Aronson, J. K. Chloroquine and hydroxychloroquine in covid-19. BMJ 369, m1432, https://doi.org/10.1136/bmj.m1432 (2020).
3. Touret, F. & de Lamballerie, X. Of chloroquine and COVID-19. Antiviral Res 177, 104762, https://doi.org/10.1016/j.antiviral.2020.104762 (2020).
4. Hoffmann, M. et al. SARS-CoV-2 Cell Entry Depends on ACE2 and TMPRSS2 and Is Blocked by a Clinically Proven Protease Inhibitor. Cell, https://doi.org/10.1016/j.cell.2020.02.052 (2020).
5. Yao, X. et al. In Vitro Antiviral Activity and Projection of Optimized Dosing Design of Hydroxychloroquine for the Treatment of Severe Acute Respiratory Syndrome Coronavirus 2 (SARS-CoV-2). Clin Infect Dis, https://doi.org/10.1093/cid/ciaa237 (2020).
6. Liu, J. et al. Hydroxychloroquine, a less toxic derivative of chloroquine, is effective in inhibiting SARS-CoV-2 infection in vitro. Cell Discov 6, 16, https://doi.org/10.1038/s41421-020-0156-0 (2020).
7. Rolain, J. M., Colson, P. & Raoult, D. Recycling of chloroquine and its hydroxyl analogue to face bacterial, fungal and viral infections in the 21st century. Int J Antimicrob Agents 30, 297-308, https://doi.org/10.1016/j.ijantimicag.2007.05.015 (2007).
8. Park, J. E. et al. Proteolytic processing of Middle East respiratory syndrome coronavirus spikes expands virus tropism. Proc Natl Acad Sci U S A 113, 12262-12267, https://doi.org/10.1073/pnas.1608147113 (2016).
9. Shirato, K., Kawase, M. & Matsuyama, S. Wild-type human coronaviruses prefer cell-surface TMPRSS2 to endosomal cathepsins for cell entry. Virology 517, 9-15, https://doi.org/10.1016/j.virol.2017.11.012 (2018).
10. Shirato, K., Kanou, K., Kawase, M. & Matsuyama, S. Clinical Isolates of Human Coronavirus 229E Bypass the Endosome for Cell Entry. J Virol 91, https://doi.org/10.1128/JVI.01387-16 (2017).
11. Iwata-Yoshikawa, N. et al. TMPRSS2 Contributes to Virus Spread and Immunopathology in the Airways of Murine Models after Coronavirus Infection. J Virol 93, https://doi.org/10.1128/JVI.01815-18 (2019).
12. Zhou, Y. et al. Protease inhibitors targeting coronavirus and filovirus entry. Antiviral Res 116, 76-84, https://doi.org/10.1016/j.antiviral.2015.01.011 (2015).
13. Matsuyama, S. et al. Enhanced isolation of SARS-CoV-2 by TMPRSS2-expressing cells. Proc Natl Acad Sci U S A 117, 7001-7003, https://doi.org/10.1073/pnas.2002589117 (2020).
14. Boulware, D. R. et al. A Randomized Trial of Hydroxychloroquine as Postexposure Prophylaxis for Covid-19. N Engl J Med, https://doi.org/10.1056/NEJMoa2016638 (2020).
15. Kupferschmidt, K. Big studies dim hopes for hydroxychloroquine. Science 368, 1166-1167, https://doi.org/10.1126/science.368.6496.1166 (2020).
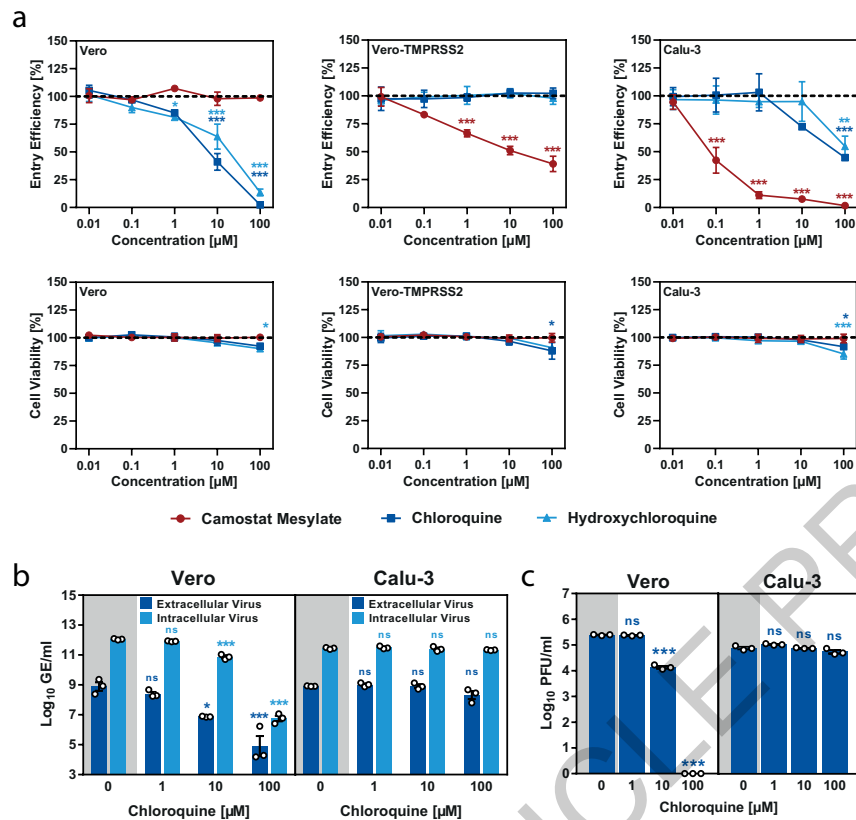
Fig. 1 | Chloroquine fails to block SARS-CoV-2 infection of human lung cells. a, Vero, Vero-TMPRSS2 and Calu-3 cells were preincubated with inhibitor (0, 0.01, 0.1, 1, 10 or 100 μM) and then inoculated with replication-defective vesicular stomatitis virus reporter particles bearing SARS-2-S followed by quantification of transduction efficiency (upper panel). Alternatively, the cells were not inoculated with virus particles but were subjected to an analysis of cell viability at the same time as transduction was quantified (lower panel). Transduction efficiency was quantified by measuring virus-encoded luciferase activity in cell lysates. Cell viability was measured using the Cell Titer Glo assay. Shown are the average (mean), normalized data (relative entry efficiency or cell viability for inhibitor-treated cells compared to untreated cells [set as 100%]) from three biological replicates (n = 3), each conducted with quadruplicate samples. **b**, Untreated or chloroquine pre-incubated Vero and Calu-3 cells were inoculated with SARS-CoV-2 Munich isolate (patient Isolate 929, BetaCoV/Munich/BavPat1/2020|EPI_ISL_406862) at an MOI of 0.001. At 24 h post inoculation, viral RNA was isolated from the culture supernatant (extracellular virus, dark blue) and the infected cells (intracellular virus, light blue), and SARS-CoV-2 genome equivalents (GE) were determined by quantitative RT-PCR. The average (mean) of three biological replicates (n=3) each conducted with single samples is shown. **c**, The experiment was conducted as described for panel b but the number of infectious SARS-CoV-2 particles in culture supernatants was determined by plaque titration on Vero cells. PFU, plaque forming units. Error bars in all panels indicate the standard error of the mean. Statistical significance was analyzed by two-way analysis of variance with Dunnett's posttest (p > 0.05, not significant [ns]; $p \leq 0.05$, *; $p \leq 0.01$, **; $p \leq 0.001$, ***). *P values* (always from left to right): panel a (Camostat Mesylate/Chloroquine/Hydroxychloroquine), pseudotype entry: Vero (0.9999/0.8587/0.9997, 0.9842/0.9846/0.3904, 0.6860/0.0991/0.0223, 0.9968/0.0001/0.0001, 0.9997/0.0001/0.0001), Vero-TMPRSS2 (0.9999/0.9968/0.9795, 0.1251/0.9962/0.9998, 0.0004/0.9997/0.9999, 0.0001/0.9967/0.9982, 0.0001/0.9981/0.9986; Calu-3: 0.9900/0.9999/0.9986, 0.0003/0.9999/0.9983, 0.0001/0.9988/0.9929, 0.0001/0.1291/0.9938, 0.0001/0.0005/0.0045); cell viability: Vero (0.9273/0.9999/0.9999, 0.9999/0.8710/0.9642, 0.9999/0.9996/0.9999, 0.9999/0.8958/0.4818, 0.9998/0.0838/0.0161), Vero-TMPRSS2 (0.9998/0.9999/0.9959, 0.9811/0.9985/0.9362, 0.9998/0.9985/0.9997, 0.9997/0.8835/0.9998, 0.9999/0.0315/0.1422), Calu-3 (0.9986/0.9999/0.9999, 0.9999/0.9997/0.9999, 0.9986/0.9999/0.8134, 0.9924/0.9275/0.7125, 0.9983/0.0492/0.0002); panel b (extracellular/intracellular): Vero (0.6844/0.6989, 0.0121/0.0002, 0.0002/0.0001), Calu-3 (0.9434/0.8800, 0.9999/0.8830, 0.0517/0.3924); panel c, Vero (0.9561, 0.0001, 0.0001), Calu-3: (0.1184, 0.9997, 0.0987).

Article

Table 1 | Half-maximal inhibitory concentrations of the drugs tested

	IC_{50} [µM]		
	Vero	Vero-TMPRSS2	Calu-3
Camostat Mesylate	n.d.	5.7	0.083
Chloroquine	6.5	n.d.	64.7
Hydroxychloroquine	13.3	n.d.	119

Methods

Cells

Vero76, Vero76 stably expressing TMPRSS2 (both used for pseudotype experiments)[4], the Vero76 subclone VeroE6 (used for SARS-CoV-2 experiments), 293T and Calu-3 cells[16] were cultivated in Dulbecco's Modified Eagle's Medium (DMEM) or Minimum Essential Medium (MEM, Calu-3) supplemented with 10% fetal bovine serum (FBS) and 1% penicillin/streptomycin. In case of Calu-3 cells, the medium was also supplemented with 1% non-essential amino acids, and 1% sodium pyruvate. All cell lines were incubated at 37 °C and 5% CO_2 and were obtained from repositories (VeroE6, 293T) or collaborators (Calu-3, Vero76). Cell lines were free of mycoplasma, authenticated based on morphology and growth properties and confirmed by PCR to be of the correct species. The cell lines used were not listed as commonly misidentified cell lines by the ICLAC register.

Production of pseudotyped particles

Vesicular stomatitis virus particles pseudotyped with SARS-2-S (VSVpp) were generated according to a published protocol[4,17]. At 24 h posttransfection, 293T cells expressing SARS-2-S were inoculated with a replication-restricted, VSV-G-trans-complemented VSV, which lacks the genetic information for VSV-G but instead codes for the reporter genes eGFP (enhanced green fluorescent protein) and FLuc (firefly luciferase), VSV*ΔG-FLuc[18], kindly provided by Gert Zimmer, Institute of Virology and Immunology, Mittelhäusern/Switzerland. After 1 h of incubation at 37 °C and 5% CO_2, the inoculum was aspirated and the cells were washed with PBS (phosphate buffered saline) before standard culture medium was added. The culture medium was further supplemented with culture supernatant from I1-hybridoma cells (CRL-2700 cells, ATCC) containing anti-VSV-G antibody (1:1,000) in order to inactivate residual input virus. Following an incubation period of 18 h at 37 °C and 5% CO_2, the culture supernatant was collected, centrifuged to pellet cellular debris, and the clarified supernatant was aliquoted and stored at -80 °C until further use.

Transduction of target cells with pseudotypes and its inhibition

For transduction experiments, target cells (Vero, Vero-TMPRSS2, Calu-3) were grown in 96-well plates to reach ~50-70% confluency. Then, cells were pre-incubated with medium containing different concentrations (10 nM, 100 nM, 1 µM, 10 µM, 100 µM) of camostat mesylate (Sigma-Aldrich), chloroquine or hydroxychloroquine (both Tocris) or DMSO (Roth, solvent control) for 2 h at 37 °C and 5% CO_2, before they were inoculated with the respective VSVpp harboring SARS-2-S. At 18 h posttransduction, culture supernatants were aspirated and cells were lysed by incubation (30 min, room temperature) with Cell Culture Lysis Reagent (Promega). Cell lysates were subsequently transferred into white, opaque-walled 96-well plates and FLuc activity was quantified as an indicator of transduction efficiency, using the Beetle-Juice substrate (PJK) and a Hidex Sense plate reader (Hidex) operated with Hidex PlateReaderSoftware (version 0.5.41.0, Hidex). Raw luminescence values (indicating luciferase activity) were recorded as counts per second. For normalization, transduction of control-treated cells was set as 100% and the relative transduction efficiencies in the presence of camostat mesylate/chloroquine/hydroxychloroquine were calculated. Transduction experiments were performed in technical quadruplicates using three separate pseudotype preparations.

SARS-CoV-2 infection and its inhibition

Virus infections were done with SARS-CoV-2 Munich isolate 929. VeroE6 or Calu-3 cells were seeded at densities of 3.5×10^5 cells/ml or 6×10^5 cells/ml in 12-well plates, respectively. After 24 h, cells were incubated with chloroquine (1, 10, 100 µM) or left untreated (control) for 1 h at 37 °C. Subsequently, cells were infected with an MOI = 0.001 in serum-free OPTIpro medium containing the above

mentioned chloroquine concentrations at 4 °C for 30 min to allow virus attachment. Afterwards, infection medium was removed and the wells were washed twice with PBS and refilled with DMEM supplemented with chloroquine as described above and incubated at 37 °C. Samples were taken at 24 h post infection. Infection experiments were conducted with biological triplicates in a biosafety level 3 laboratory.

Viral RNA extraction and real-time reverse-transcription PCR

For viral RNA extraction from supernatants, 50 µl of cell culture supernatant was mixed with RAV1 lysis buffer (Macherey&Nagel) followed by an incubation at 70 °C for 10 min. RNA extraction was performed as recommended by the manufacturer (Macherey&Nagel). For intracellular viral RNA extraction, cells were washed with PBS and lysed with Trizol (Zymo). SARS-CoV-2 genome equivalents were detected by real-time RT-PCR assay targeting SARS-CoV-2 E gene as reported before[19], using the following primers: E_Sarbeco_F: ACAGGTACGTTAATAGTTAATAGCGT; E_Sarbeco_P1: FAM-ACACTAGCCATCCTTACTGCGCTTCG-BBQ; E_Sarbeco_R: ATATTGCAGCAGTACGCACACA. Real-time RT-PCR experiment and data processing was done using the LightCycler® 480 Real-Time PCR System (Roche) and LightCycler® 480 Software (version 1.5, Roche Molecular Systems). Absolute quantification was performed using SARS-CoV-2-specific in vitro-transcribed RNA standards, as described before.

Plaque assay

Infectious SARS-CoV-2 plaque forming units (PFU) were quantified by plaque titration on VeroE6 cells, as described previously[20], with minor modifications. VeroE6 monolayers were seeded in 24-well plates, washed with PBS, incubated with serial dilutions of SARS-CoV-2-containing cell culture supernatants in duplicates, and overlaid with 1.2% Avicel in DMEM, supplemented as described above. After 72 h, cells were fixated with 6% formaline and visualized by crystal violet staining.

Cell viability assay

The cell viability was quantified using the CellTiter-Glo assay (Promega) and employing the same experimental conditions as used for transduction experiments with the exception that cells were not inoculated with virus particles. In brief, cells were preincubated for 2 h at 37 °C and 5% CO_2 with medium containing different concentrations (10 nM, 100 nM, 1 µM, 10 µM, 100 µM) of camostat mesylate, chloroquine or hydroxychloroquine, or DMSO (solvent control), before standard culture medium was added (instead of VSVpp) and cells were further incubated for 18 h. Next, intracellular adenosine triphosphate levels were quantified as an indicator of cell viability. For this, culture supernatants were aspirated and cells were lysed by incubation with CellTiter-Glo substrate for 30 min at room temperature. Cell lysates were subsequently transferred into white, opaque-walled 96-well plates and luminescence was measured using a Hidex Sense plate reader (Hidex). Luminescence values (indicating cell viability) were recorded as absolute counts over a period of 200 msec/well. For normalization, cell viability of control-treated cells was set as 100% and the relative viability of cells incubated in the presence of camostat mesylate/chloroquine/hydroxychloroquine was calculated. Cell viability experiments were performed in technical quadruplicates and repeated with three separately-prepared dilution series of the inhibitors.

Statistical analysis

Two-way analysis of variance (ANOVA) with Dunnett's posttest was performed to analyze statistical significance of differences in (i) transduction efficiencies, (ii) SARS-CoV-2 genome equivalents or (iii) SARS-CoV-2 titers between control- and inhibitor-treated cells ($p > 0.05$, not significant [ns]; $p \leq 0.05$, *; $p \leq 0.01$, **; $p \leq 0.001$, ***). Inhibitory concentration 50 (IC_{50}) values, which indicate the inhibitor

Article

concentration leading to 50% reduction of transduction were calculated using a non-linear regression model with variable slope. Statistical analyses and IC_{50} calculations were performed using GraphPad Prism (version 8.4.2).

Reporting summary

Further information on research design is available in the Nature Research Reporting Summary linked to this paper.

Data availability

All data are provided within the paper and associated online files. Source data are provided with this paper.

16. Klemm, C. *et al*. Mitogen-activated protein kinases (MAPKs) regulate IL-6 over-production during concomitant influenza virus and Staphylococcus aureus infection. *Sci Rep* **7**, 42473, https://doi.org/10.1038/srep42473 (2017).
17. Kleine-Weber, H. *et al*. Mutations in the Spike Protein of Middle East Respiratory Syndrome Coronavirus Transmitted in Korea Increase Resistance to Antibody-Mediated Neutralization. *J Virol* **93**, https://doi.org/10.1128/JVI.01381-18 (2019).
18. Berger Rentsch, M. & Zimmer, G. A vesicular stomatitis virus replicon-based bioassay for the rapid and sensitive determination of multi-species type I interferon. *PLoS One* **6**, e25858, https://doi.org/10.1371/journal.pone.0025858 (2011).
19. Corman, V. M. *et al*. Detection of 2019 novel coronavirus (2019-nCoV) by real-time RT-PCR. *Euro Surveill* **25**, https://doi.org/10.2807/1560-7917.ES.2020.25.3.2000045 (2020).
20. Herzog, P., Drosten, C. & Muller, M. A. Plaque assay for human coronavirus NL63 using human colon carcinoma cells. *Virol J* **5**, 138, https://doi.org/10.1186/1743-422X-5-138 (2008).

Corresponding author(s):   Markus Hoffmann, Stefan Pöhlmann

Last updated by author(s):   Jun 29, 2020

Reporting Summary

Nature Research wishes to improve the reproducibility of the work that we publish. This form provides structure for consistency and transparency in reporting. For further information on Nature Research policies, see our Editorial Policies and the Editorial Policy Checklist.

Statistics

For all statistical analyses, confirm that the following items are present in the figure legend, table legend, main text, or Methods section.

n/a	Confirmed	
☐	☒	The exact sample size (*n*) for each experimental group/condition, given as a discrete number and unit of measurement
☐	☒	A statement on whether measurements were taken from distinct samples or whether the same sample was measured repeatedly
☐	☒	The statistical test(s) used AND whether they are one- or two-sided *Only common tests should be described solely by name; describe more complex techniques in the Methods section.*
☐	☒	A description of all covariates tested
☐	☒	A description of any assumptions or corrections, such as tests of normality and adjustment for multiple comparisons
☐	☒	A full description of the statistical parameters including central tendency (e.g. means) or other basic estimates (e.g. regression coefficient) AND variation (e.g. standard deviation) or associated estimates of uncertainty (e.g. confidence intervals)
☐	☒	For null hypothesis testing, the test statistic (e.g. F, t, r) with confidence intervals, effect sizes, degrees of freedom and P value noted *Give P values as exact values whenever suitable.*
☒	☐	For Bayesian analysis, information on the choice of priors and Markov chain Monte Carlo settings
☒	☐	For hierarchical and complex designs, identification of the appropriate level for tests and full reporting of outcomes
☒	☐	Estimates of effect sizes (e.g. Cohen's *d*, Pearson's *r*), indicating how they were calculated

Our web collection on statistics for biologists contains articles on many of the points above.

Software and code

Policy information about availability of computer code

Data collection	- Hidex Sense Microplate Reader Software (version 0.5.41.0), Hidex Deutschland Vertrieb GmbH, https://www.hidex.de/ - LightCycler® 480 Software (version 1.5), Roche Molecular Systems, Inc., https://lifescience.roche.com/
Data analysis	- GraphPad Prism (version 8.4.2), GraphPad Software, https://www.graphpad.com/

For manuscripts utilizing custom algorithms or software that are central to the research but not yet described in published literature, software must be made available to editors and reviewers. We strongly encourage code deposition in a community repository (e.g. GitHub). See the Nature Research guidelines for submitting code & software for further information.

Data

Policy information about availability of data

All manuscripts must include a data availability statement. This statement should provide the following information, where applicable:
- Accession codes, unique identifiers, or web links for publicly available datasets
- A list of figures that have associated raw data
- A description of any restrictions on data availability

All source data are available within the paper.

Field-specific reporting

Life sciences study design

All studies must disclose on these points even when the disclosure is negative.

Sample size	No sample size calculations were performed. Sample sizes adhere to standards in the fied; for instance, three biological replicates performed with technical replicates.
Data exclusions	No data were excluded from the analysis.
Replication	All findings were confirmed in three independent experiments. All results could be reproduced.
Randomization	Experiments were performed in vitro with standard immortalized cell lines. Therefore, no randomization was required.
Blinding	No groups were allocated. Therefore, blinding was not necessary.

Reporting for specific materials, systems and methods

We require information from authors about some types of materials, experimental systems and methods used in many studies. Here, indicate whether each material, system or method listed is relevant to your study. If you are not sure if a list item applies to your research, read the appropriate section before selecting a response.

Materials & experimental systems

n/a	Involved in the study
✗	Antibodies
	✗ Eukaryotic cell lines
✗	Palaeontology and archaeology
✗	Animals and other organisms
✗	Human research participants
✗	Clinical data
✗	Dual use research of concern

Methods

n/a	Involved in the study
✗	ChIP-seq
✗	Flow cytometry
✗	MRI-based neuroimaging

Eukaryotic cell lines

Policy information about cell lines

Cell line source(s)	- Vero76: Provided by Andrea Maisner (Philipps University Marburg, Marburg/Germany) - Vero76-TMPRSS2: Generated from parental Vero76 cells by retroviral transduction (Hoffmann et al., 2020) - VeroE6: Obtained from ATCC (CCL-81) - Calu-3: Provided by Stephan Ludwig (Institute of Virology (IVM), Westfaelische Wilhelms-University Muenster) and initially obtained from ATCC -293T: Obtained from DSMZ (ACC 635)
Authentication	Species origin of all cell lines was confirmed by sequencing a PCR-amplified fragment of the cytochrome c oxidase gene. Cell lines were further authenticated by analysis of morphology and growth properties.
Mycoplasma contamination	Cells were tested for the presence of mycoplasma by PCR. No contamination by mycoplasma was detected.
Commonly misidentified lines (See ICLAC register)	The used cell lines are not listed as commonly misidentified cell lines by the ICLAC register.